Internal Report IASF-BO 348/2002

September 2002

SIMULATION OF GALACTIC POLARIZED SYNCHROTRON MAPS

C. Zampolli and C. Burigana

IASF/CNR - Sezione di Bologna
Via P. Gobetti 101, I-40129 Bologna, Italy

Internal Report IASF-BO 348/2002

September 2002

SIMULATION OF GALACTIC POLARIZED SYNCHROTRON MAPS

C. Zampolli and C. Burigana

IASF/CNR - Sezione di Bologna
Via P. Gobetti 101, I-40129 Bologna, Italy

SUMMARY – We present methods to simulate maps of polarized Galactic synchrotron emission using the information provided by the Leiden surveys and the Parkes and Effelsberg surveys and some preliminary results. The large sky coverage of the Leiden surveys, although at low resolution, has been exploited in order to simulate all-sky maps of polarized synchrotron emission by implementing a geometric algorithm based on central symmetries in order to fill the unobserved sky region. Four different models of maps of simulated fluctuations at small angular scales have been generated by taking advantage from the best fit values of the power law parametrization found by Baccigalupi et al. 2001 for the angular power spectra of some small regions extracted from the Parkes and Effelsberg surveys at high resolution. The small angular scale fluctuation maps have been then superimposed to the large scale fluctuation map, resulting in four different models of all-sky simulations of the polarized Galactic synchrotron component in the microwave frequency range.

1 Introduction

The level of CMB polarization and the shape of the angular power spectrum of its polarization fluctuations can be calculated through detailed Boltzmann codes according to the current cosmological models. The accurate measurement of this spectrum will be crucial in order to study the properties of the primordial density fluctuations and the history of the Universe.

To assess the reliability of the CMB polarization measurements from future satellite missions such as PLANCK and to optimize them, it is necessary to study the instrumental systematic effects and to outline the best data analysis technique, carring out numerical simulations of the observations. Simulation activities should exploit the existing observations of the sky in the range of the microwave and/or in the nearby bands, in order to forecast some properties of the real sky in regions and at frequencies that have not been explored yet. This type of work is the basis of quite realistic simulations of the observations from space missions, crucial for a proper analysis of the data, when they will be available.

The Galactic polarized diffuse synchrotron emission will be the most relevant foreground in CMB polarization experiments at frequencies $\nu \leq 50 \div 100$ GHz on large and intermediate angular scales ($l \lesssim 100$). For this reason, the development of methods to simulate all-sky maps of this component is very useful for present and future polarization experiments.

1.1 Theoretical framework - An existing model

An all-sky model of the Galactic polarized diffuse synchrotron emission has been developed by Giardino et al. 2002 starting from the Parkes survey at 2.4 GHz, the Haslam survey at 408 GHz, the Reich & Reich survey at 1420 GHz, and the Jonas survey ay 2326 MHz. The model has been used to produce maps at 30 and 100 GHz. It assumes that the polarized component of the synchrotron emission in a given direction is proportional to the non-polarized intensity according to the equations

$$Q = fT\cos(2\theta), \quad (1)$$

$$U = fT\sin(2\theta), \quad (2)$$

where θ is the polarization angle and T is the brightness temperature; its dependence on the frequency is quite well described by a power law $T(\nu) \propto \nu^{\beta}$, where β is the antenna temperature spectral index ($\beta \sim -2.9$).

Although very useful for simulation activities, in particular to assess worst case scenarios for Galactic foreground contamination, the model of polarized emission simulated by Giardino et al. 2002 links the brightness temperature T and the Stokes parameters Q and U and does not take into account crucial differences between the temperature and the polarization pattern, so predicting a structure marked on the Galactic plane, not observed in the available surveys. In fact, while T is a scalar quantity that derives from the integral along the line of sight (and inside the beam angular region), polarization is a vectorial quantity, and as a consequence, its integral along the line of sight (and inside the beam) strictly depends on the signal coherence properties in the superposition of the various contributes. As a result, a compensation mechanism arises on large linear distances and inside the beam, and an effective signal superpositon is limited to just some kpcs.

1.2 Towards a model based on polarization surveys

In this work we present methods to simulate maps of Galactic diffuse polarized synchrotron emission maximizing the use of the information provided by the polarization surveys on large and small angular scales, as well as some preliminary results. We carried out our study first

on large and then on small scales, in order to obtain polarized emission maps that could provide information on both small and large multipoles l, crucial for simulation activities related to a whole sky and high resolution experiment such PLANCK/LFI.

The maps of large scale fluctuations have been produced with a geometric algorithm, based on central symmetries, using as starting point the maps obtained by Burigana and La Porta 2002. For the small angular scales, we started from the results obtained by Baccigalupi et al. 2001. In particular, we have realized all-sky simulations of the distribution of the parameters describing the synchrotron angular power spectrum at large multipoles l ($C_l \propto \alpha l^{\beta}$).

Then, the maps simulated on large and small scales have been superimposed in order to obtain overall synchrotron emission simulated maps.

2 Large scale maps

The Galactic polarized diffuse synchrotron emission will be one of the major astrophysical contamination sources at small and intermediate multipoles in the experiments on the CMB polarization anisotropies in the frequency range $\nu < 50 \div 100$ GHz. At the frequencies around 1 GHz, the Galactic synchrotron emission dominates over the bremsstrahlung emission that is only weakly polarized. The study of the Galactic synchrotron emission makes it possible to get important information on the properties of the Galactic magnetic field and of the ionized interstellar matter.

While waiting for the results of experiments (in progress and in the future) characterized by high sensitivity and resolution that will cover wide sky areas at different Galactic latitudes and different frequencies, we can exploit the information provided by the Leiden surveys, that cover about the 50% of the sky. From these surveys, it is possible to obtain the angular power spectrum of the Galactic polarized diffuse radio emission at frequencies between 408 and 1411 MHz, observed with a (FWHM) resolution between 2.3° and 0.6°, respectively.

2.1 Maps from the Leiden surveys

The maps that have been used for our simulation activity have been realized from the Leiden surveys, which observe quite different sky regions. The pixel size of these maps is $\gtrsim 0.92°$.

Within the surveys, it is possible to identify regions that are better sampled than the others, at low and middle-high Galactic latitudes. Burigana & La Porta 2002 have extracted three patches:

-patch 1 : $110° \leq l \leq 160°, 0° \leq b \leq 20°$;

-patch 2 : $5° \leq l \leq 80°, b \geq 50°$ and $0° \leq l \leq 5°, b \geq 60°$;

-patch 3 : $10° \leq l \leq 80°, b \geq 70°$.

The polarized signal in these patches, and therefore the signal-to-noise ratio also, is typically higher than the average. Thanks to their angular extension θ^2, the angular resolution and the sensitivity of the measurements, from these patches it is possible to study the C_l^{ant} (here in terms of antenna temperature) in a multipole range from $l \simeq 20 \div 30$ (corresponding to angular scales $\sim few \times 180°/\theta$, where the boundary effects do not affect significantly the analysis), to $l \sim 100$, where, also for these better sampled regions, the noise and signal powers become comparable.

The main problem one faces analyzing the Leiden surveys is due to their very poor sky sampling. As a consequence, many discontinuity effects could be produced on pixel size scales. The maps generated by Burigana & La Porta 2002 are the result of an interpolation

method and a resolution choice ($\sim 0.92°$) aimed to solve these problems; from these maps, it is possible to get reliable information only on scales $\gtrsim 2°$ ($l \lesssim 100$) considering the patches, and on scales $\gtrsim 4°$ ($l \lesssim 100$) working on the whole region covered by the surveys.

The maps of P, Q, and U obtained by Burigana & La Porta 2002 have been exploited to derive the polarized signal angular power spectrum, both for the whole survey and for the three patches, using the *anafast* code from the software package HEALPix (Górski et al. 1998), and renormalizing then the C_l^{ant} to the case of an all-sky coverage according to the relation:

$$C_l^{allsky} = C_l^{patch} \times \frac{n_{pixel}^{all\ \ sky}}{n_{pixel}^{patch}}. \qquad (3)$$

Preliminar results at 1411 MHz and tests on the validity of the method extensively discussed by Burigana & La Porta 2002 to get the C_l^{ant} from patches with relatively small dimensions have been previously reported in Baccigalupi et al. 2001: the spectrum obtained in this way is found to be in a good agreement with that obtained at the same frequency in a partially coincident sky region from the survey by Uyaniker et al. 1999 that shows a much better sensitivity and sky sampling.

2.2 Angular power spectrum and noise in the starting maps

The angular power spectrum derived from each map is mainly due to the sum of the diffuse synchrotron emission, the most important astrophysical component in the considered frequency range, and to the instrumental noise; in particular, the latter dominates at large multipoles as evident from the flattening of the angular power spectrum. The two components that make up the reconstructed C_l^{ant}s have been fitted by Burigana & La Porta 2002. The fit parameters depend on ν and on the considered sky region.

The level of the noise angular power spectrum derived from the fit is in good agreement with that extracted from simulated maps of white noise produced in three different ways on the basis of the rms noise in each map pixel. By analysing the whole survey maps, no information can be obtain at multipoles larger than $l \sim 50$. On the contrary, for what concerns the three considered patches, the power of the noise spectrum is much smaller than that derived from the signal map, indipendently of the considered case, up to $l \sim 100$. This confirms that not only from the point of view of the sky sampling, but also from the point of view of the sensitivity, the three patches can be used to extract the C_l^{ant} up to $l \sim 100$.

From the analysis of the whole coverage it is possible to get reliable information also at $5 \leq l \leq 30$ (obviously, only nearly full sky observation can provide reliable information at lower multipoles). In this case, both the noise and all the possible effects due to the poor sampling or to the interpolation technique adopted by Burigana & La Porta 2002 can be neglected. What results is a flattening of the spectrum compared to that at the high multipoles; the slope at $\nu = 1411$ MHz, of crucial importance for the extrapolation to higher frequencies, is close to -2.5. This results in a nearly flat behaviour of the temperature fluctuations $\delta T_l = \sqrt{l(2l+1)C_l/4\pi}$ at $5 \leq l \leq 30$.

As regards the synchrotron angular power spectrum at multipoles between $\lesssim 30$ and $\lesssim 100 \div 200$, slopes varying from about -3 to about $-1 \div -1.5$ have been found, mainly depending on the frequency albeit also on the considered sky region.

2.3 Frequency dependence

Thanks to their large sky coverage ad to their frequency coverage, the Leiden surveys offer the opportunity to study the dependence of the polarized Galactic synchrotron signal on the frequency ν. Obviously, depolarization effects and possible transitions from essentially

optically thin regimes to significantly self-absorbed ones could hide the intrinsic spectral synchrotron behaviour.

A large variation of the spectral index among different sky pixels is found, probably due to true variations of the index itself, but also to the limited sensitivity and to other, not well understood, effects in the data.

The spectral indices observed at $l = 50$ (a value that can be considered representative for this kind of analysis) are ~ -3.2 (from the whole coverage analysis), -3.3 (patch 1), -3.6 (patch 2), and -3.9 (patch 3). At the highest frequencies (820 and 1411 MHz), crucial for the extrapolation at frequencies of $20 \div 30$ GHz (where CMB polarization anisotropy experiments are on-going and planned), beamwidth depolarization effects are expected to be similar and the observed slope can be easily explained assuming an intrinsic index of -5.8 (-0.9 in terms of flux) and a depolarization due to Faraday rotation with a RM of about 15 rad/m^2.

2.4 All-sky simulated maps on large scales

As previosly explained, the Leiden surveys cover about half of the sky with a poor sampling. As a consequence, the reconstruction of the angular power spectrum is limited to the range $5 \leq l \leq 50$ for the whole survey, and to the range $30 \leq l \leq 100$ for the three patches with sampling better than the average. On-going and future experiments will observe nearly the full sky with a good sampling, so assuring a statistical and scientific information of considerable importance.

2.4.1 The filling algorithm

The approach of our algorithm designed to obtain full-sky maps from a partial sky coverage (provided by the maps obtained from the Leiden surveys as described aboved) is geometric. To first approximation, we can describe it as an application of the central symmetry, given a choice of a symmetry centre. However, since the initial region is neither uniform nor regular, and since it corresponds to about the 45% of the whole sky (22304 full pixels out of a total of 49152 in a map created with the package HEALPix at resolution $n_{side} = 64$, that means with pixels of about 1°), a single application of this procedure does not allow to cover the whole sky. For example, using as symmetry centre the centre of the sphere of unit radius (the point with (0, 0, 0) coordinates) and associating to each unobserved pixel the value corresponding to that simmetrically located with respect to him, did not assure to reach the 100% of covered sky. In order to solve this problem, we have generated the filling algorithm described here below.

- **step 1: determination of the "barycentre"**

  The first phase consists in finding the coordinates of the "barycentre" of the initial region, defined as the point with the mean coordinates $(\bar{x}, \bar{y}, \bar{z})$ of the region initially covered.

- **step 2: choice of the first penetration parameter and of the first symmetry centre**

  Let's define *penetration parameter* the distance between the centre of the sphere **O** and the symmetry centre **S** along the line connecting the centre **O** and the point **S**.

  This step of the algorithm consists in choosing how much to move towards the barycentre found in the previous step, starting from the centre **O** = (0, 0, 0), in order to determine an optimum symmetry centre. It is worth to note that, the greater the distance from the centre of the sphere towards the surface, the wider the extension of the originally uncovered sky region that can be reached, and, as a consequence, filled; at

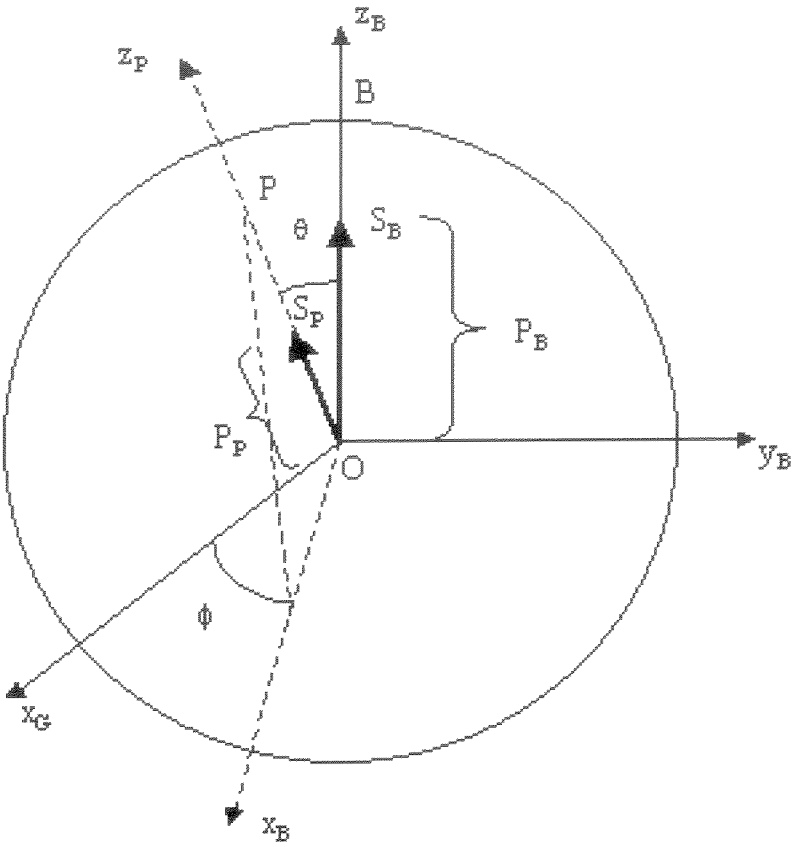

Figure 1: The figure shows the celestial sphere. The axes x_B, y_B e z_B are the cartesian axes of the barycentre reference system. The point B is the barycentre itself; S_B is the first symmetry centre, P_B the first penetration parameter; the angles θ and ϕ are the polar spherical coordinates of P ($r = 1$), that is one of the four points determined by the user that will be then used for the other symmetries; P_P is the second penetration parameter (see also the text).

the same time, the smaller the portion of the initial region that is used in the symmetry, and the larger the stretching deformation, because the value of a pixel originally observed is attributed to more than one pixel originally unobserved. For this reason, the chosen value of the penetration parametr has to be significantly less than unity.

Since even by considering different penetration parameters inside the sphere it is not possible to fill the whole unobserved sky region, we need to use other (four) new symmetry centres.

- **step 3: second penetration parameter choice**

  In this step, the user fixes the second penetration parameter from the celestial centre towards the four new points, chosen in the next step, bearing in mind that the farther from the centre of the sphere, the nearer to the borders of the initial coverage the new centres will be.

- **step 4: determination of the new further points**

  The user chooses four new pairs of Galactic coordinates θ and ϕ through which four new points are determined in the barycentre reference system. The cartesian coordinates of these points in the Galactic reference system are:

$$x = \sin\theta\cos\phi\cos\theta_b\cos\phi_b - \sin\theta\sin\phi\sin\phi_b + \cos\theta\sin\theta_b\cos\phi_b$$

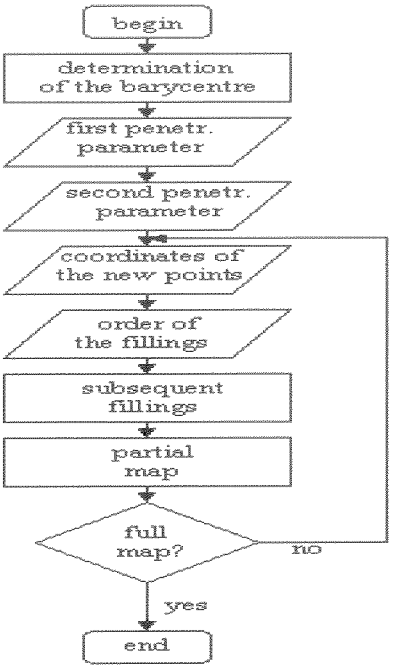

Figure 2: Flow chart of the algorithm implemented in the generation of the polarized diffuse synchrotron emission map on large scales (see also the text).

$$
\begin{aligned}
y &= \sin\theta\cos\phi\cos\theta_b\cos\phi_b - \sin\theta\sin\phi\sin\phi_b + \cos\theta\sin\theta_b\sin\phi_b \\
z &= -\sin\theta\sin\phi\sin\theta_b + cos\theta\cos\theta_b,
\end{aligned}
$$

where θ_b and ϕ_b are the barycentre Galactic coordinates. Towards these points one then moves (from the Galactic centre) of the quantity estabilished at step 3 in order to determine the four new symmetry centres.

It is worth to emphasize that, in fact, the arbitrariness of the choice reduces the artificial symmetry properties of this type of algorithm.

- **step 5: order of the symmetries and realization of the fillings**

  Therefore, the possible central symmetries to be realized starting from the initial data are five. They can be carried out in any order, since the choice of the parameter that determines their centres are independent from the consecutive fillings (obviously, going on with a new symmetry, the results of the previous one are taken into account, and a pixel already filled up is no more considered empty, but, in case, used to fill up another empty pixel). In this step, the order of the five symmetries is fixed. Then, the five consecutive fillings can be carried out.

- **step 6: check of the sky portion covered in the final map**

  If only one algorithm application is not enough to cover the whole celestial sphere, it is possible to choose the spherical coordinates for other four points, to be used as new centres in a next cycle, starting, in this case, from the map obtained in the previous one. This means, in other words, going back to step 3.

The parameters used in the map production have been:

1. penetration from the sphere centre to the mean point of the initial region = 0.1;

2. penetration from the sphere centre to the four new symmetry centres = 0.1.

It is worth to stress that the values 1. and 2. represent the ratio between the radial distances of the points on the sphere surface (mean point of the initial coverage, and arbitrary points) and those of the corresponding symmetry centres.

2.4.2 Structure removal

Although this algorithm allows to build a full-sky realistic map of the emission from the Galaxy, being based only on real data, its major disadvantage is the possible replication of particular structures of the initial map, because of the adopted central symmetry technique.

The initial map shows several regions where the Galactic signal is particularly higher than the typical signal. In particular, it is possible to identify such structures (usually called spurs) in the following regions: $70° \leq l \leq 180°$ with $-20° \leq b \leq 30°$ near the Galactic plane; $0° \leq l \leq 20°$ with $10° \leq b \leq 80°$ and $320° \leq l \leq 360°$ with $45° \leq b \leq 80°$, that together form the North Galactic Spur. The presence of such structures accounts for the fact that, when applying the algorithm described in Sect. 2.4.1, we obtain a map with very similar structures in regions approximately at: $286° \leq l \leq 360°$ with $-36° \leq b \leq 27°$ and $189° \leq l \leq 211°$ with $-81° \leq b \leq -18°$. Clearly, this result is not very reliable: the presence of other regions with high polarized Galactic emission, with signal similar to those characterizing the features discussed above, is clearly plausible, but it is quite difficult that they show the geometrical regularity in the sky produced by the application of the adopted algorithm. To avoid, or reduce, this problem, a second all-sky map has been produced by applying a suitable clockwise rotation about the longitudinal Polar Galactic axis to the map produced as described before. After having selected the regions with an excessive similarity to the spurs of the original map, we have replaced them with the signal produced in the second, rotated, all-sky map. The rotation angle (70°) has been chosen in order to reduce as long as possible in the final all-sky map the signs of the regularity and symmetry typical of the algorithm. However, a slight discontinuity remains visible at the borders of the replaced regions. Although this effect does not alter the fundamental statistical information contained in the map and is not particularly critical in the applications described in the next sections, in the future we will try to improve our algorithm in order to reduce this effect.

2.4.3 The final all-sky map

The Galactic synchrotron signal is affected by the Faraday depolarization that can be quantified in terms of the rotation measure RM. This introduces a reduction of the original signal value, P_0, described by the law

$$P(\lambda) = P_0 \frac{\sin(\lambda^2 \times \mathrm{RM})}{\lambda^2 \times \mathrm{RM}},$$

where the rotation measure RM in expressed in radians, and λ is the wavelength of observation. To produce a full sky map corrected for this effect we then multiply the map derived as described in previous sections by the corresponding corrective factor $P/P_0 = 1.083$ (with $\nu = c/\lambda = 1.4$ GHz and RM = 15 rad m^{-2}). The final step of this phase of simulation activity has been to change the map resolution from a pixel size of $\simeq 0.92°$ to a pixel size of $\simeq 3.5'$ in order to be able, then, to work with the same higher resolution maps including small scale fluctuations.

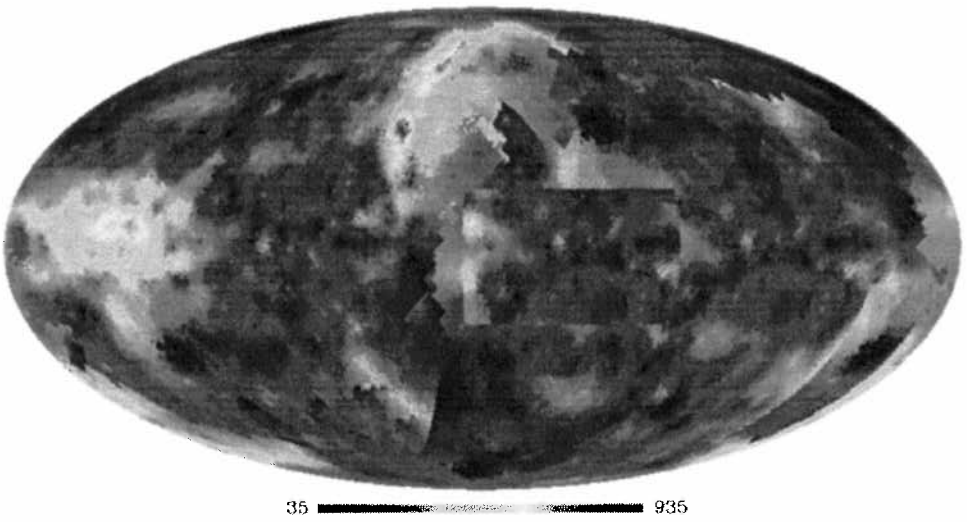

Figure 3: Large scale fluctuation map of the polarized Galactic synchrotron emission at 1.4 GHz simulated on the whole sky, at $n_{side} = 1024$.

3 The small scale fluctuations

We have generated four fluctuation models on small scale ($\sim 3.5'$), starting from the study by Baccigalupi et al. 2001 of the Parkes survey at 2.4 GHz (see Duncan 1995, Duncan 1997), of the Effelsberg survey at 2.7 GHz (see Duncan 1999), and at 1.4 GHz, that cover regions as far as $\pm 20°$ of Galactic latitude (see Uyaniker et al. 1998 and Uyaniker et al. 1999).

3.1 Polarization survey

High resolution polarization surveys of sky regions around the Galactic plane have been recently realized and studied by Duncan et al. 1997 (D97) and Duncan et al. 1999 (D99) at 2.4 and 2.695 GHz respectively. Instead, Uyaniker et al. 1999 (U99) have realized a temperature and polarization survey of four regions at medium Galactic latitudes (to $b = 20°$) at 1.4 GHz. All these data, with technical details, can be found at the web site `http://www.mpifr-bonn.mpg.de/survey.html`.

3.1.1 D97

The survey covers 127° in Galactic latitude ($238° < l < 5°$) to at least $b \pm 5°$ (for $340° < l < 5°$, the survey extends to $b = +7°$, for $340° < l < 352°$ to $b = -7°$, and for $240° < l < 270°$ to $b = 8°$) with an angular resolution of $10.4'$. The total area amounts to $\simeq 1413$ square degrees. The central frequency is 2.417 GHz, and the bandwidth is about 145 MHz. The nominal rms noise in total power is 17 mJy/beam (that is 8 mK), and 11 mJy/beam (that is 5.3 mK) in polarization; it is worth to say that a lower rms of 11 mJy/beam in total intensity and 6 mJy/beam in polarization has been achieved over the $\simeq 43\%$ of the total area. The values of Stokes parameters Q and U and the temperature total intensity are given on a rectangular grid every $4'$ in units of mJy/beam; the conversion factor to brightness temperature is 1 mJy/beam area = 0.48 mK (Duncan, private communication).

3.1.2 D99

D99 reports the polarimetric data from the Effelsberg survey at 2.695 GHz, with $\theta_{FWHM} = 4.3'$ in the first Galactic quadrant. Maps at a resolution of $5.1'$ have been produced for the region $4.9° \leq l \leq 74°$, $|b| \leq 5°$, with a rms noise of 2.5 mJy/beam, corresponding to 9 mK.

3.1.3 U99

This survey has a central frequency of 1.4 GHz and has been realized at medium Galactic latitudes (to $b = 20°$). It includes four observational areas covering about 1050 square degrees: one of these is located in the first Galactic quadrant ($45° \leq l \leq 55°$, $4° \leq b \leq 20°$); the second concerns the northern part ($65° \leq l \leq 95°$, $5° \leq b \leq 15°$) and the southern part ($70° \leq l \leq 100°$, $-15° \leq b \leq -5°$) of the Cygnus region; the third, characterized by a high polarized signal, is the so-called *fan region* ($140° \leq l \leq 153°$, $3.5° \leq b \leq 10°$); last, an anticentre region ($190° \leq l \leq 210°$, $3.8° \leq b \leq 15°$). The rms noise is about 15 mK in total intensity and about 8 mK in linear polarization. The angular resolution is $9.35'$.

The Galactic diffuse emission maps have been obtained by Baccigalupi et al. 2001 subtracting from the sum of the maps the isotropic component due to the CMB and to the contributes of the unresolved extragalactic sources, for which a temperature $T_{A,isot} = 2.9$ K has been assumed.

3.1.4 Survey properties

A comparison between total emission and polarization maps shows little correlation, both for D97, for D99 and for U99. This is due to two main reasons. On one hand, there are many bright sources on the Galactic plane that are unpolarized HII regions; from these, a high thermal emission is expected. As a consequence, these regions can not provide an angular power spectrum representative of that of the synchrotron also at high Galactic latitudes. On the other hand, differential Faraday rotation or possible variations in the magnetic field orientation can cause a strong depolarization of the emission from far Galactic regions (see Burn 1996 and Duncan et al. 1999). As a result, only the polarized emission of local origin coming from a region that extends to some Kpc can be observed.

The two factors may act together: an emitting electron density variation can lead to a large enough differential Faraday rotation to cause a consistent depolarization; at the same time, the magnetic field could be distorted by turbolent motions of the ionized gas, producing a further depolarization.

For the study of the total and polarized emission, Baccigalupi et al. 2001 have put all the maps on the same grid of $12' \times 12'$. The distributions both of the total and of the polarized emission show significant deviations from the Gaussianity.

3.1.5 The angular power spectra

The study of the angular power spectra of temperature and polarization intensity ($P = \sqrt{Q^2 + U^2}$) of D97, D99, and U99 has been carried out by Baccigalupi et al. 2001 by using a spherical harmonic expansion. After projecting the surveys onto a sphere initially null anywhere, they have computed the angular power spectra using the *anafast* code of the HEALPix package; the rescaling to the case of full sky coverage has been then made by dividing by the fraction of sky coverage using Eq. 3.

In order to obtain the coefficient of the real power spectrum from the measured ones, C_l^{map}, the authors have jointly taken into account the instrumental noise and the detector

response function:

$$C_l = \frac{C_l^{map} - C_l^{noise}}{W(l)}, \quad W(l) = b(l)^2 .$$

The beam window function for each multipole is well modelled by a law of the form

$$b(l) = \exp[-l(l+1)\sigma_{beam}^2/2], \tag{4}$$

where $\sigma_{beam} = \mathrm{FWHM}/\left(2\sqrt{2\ln 2}\right)$ and FWHM is expressed in radians. In D97 the beam is slightly elliptical, and Eq. 4 has been consequently modified.

The instrumental noise has been approximated by Baccigalupi et al. 2001 with a flat power spectrum [1]:

$$C_l^{noise} = 4\pi \frac{\sigma_{noise}^2}{N_{pixels}}.$$

For D97, D99 and U99 the values of the instrumental noise are given by the authors.

The authors have analyzed some patches $10^\circ \times 10^\circ$ taken from the surveys D97, D99 and U99, from which, thanks to their dimensions, the angular power spectra could be estimated from a minimum multipole $l_{min} \simeq 100$ corresponding to an angular scale of about 2°, to a maximum multipole $l_{max} \simeq 800$. The power spectra obtained in this way have been fitted with a power law of the form:

$$C_l = \alpha l^\beta \tag{5}$$

The best fit values with the associated errors are reported in Baccigalupi et al. 2001

From D99 the authors have selected five patches centred in $l = 25^\circ, 35^\circ, 45^\circ, 55^\circ$ e 60°, near the Galactic plane, at $-5^\circ \leq b \leq 5^\circ$.

The central values and the amplitudes of regions 1, 2 and 3 from U99 are:

1. $l = 50^\circ, b = 12^\circ, \Delta l = 10^\circ, \Delta b = 15^\circ$,
2. $l = 146.4^\circ, b = 6.8^\circ, \Delta l = 12^\circ, \Delta b = 6.3^\circ$,
3. $l = 196.8^\circ, b = 11.2^\circ, \Delta l = \Delta b = 6.7^\circ$.

The mean power spectrum of the studied regions can be properly described with a power law of the form:

$$C_l^P = (1.2 \pm 0.8)10^{-9} \times \left(\frac{l}{450}\right)^{-1.8\pm0.3} \times \left(\frac{\nu}{2.4\mathrm{Ghz}}\right)^{-5.8} \mathrm{K}^2.$$

3.2 Production of small scale fluctuation maps

From the survey described in Sect. 3.1 maps of small scale fluctuation have been produced. These maps have then been summed to the low resolution Galactic synchrotron map (see Sect. 2.4) in order to obtain simulations of the polarized emission of this component.

3.2.1 Coefficient map generation

As described in Sect. 3.1, 20 patches $10^\circ \times 10^\circ$ have been extracted from D97, D99 and U99 surveys. From them, the angular power spectrum of the total and polarized intensity have been computed between $l_{min} \simeq 100$ and $l_{max} \simeq 800$. In particular, the C_ls have been fitted with a power law (see Eq. 5) whose coefficient assumed different values according to the considered patch.

[1] We remember that the power spectra reported here are rescaled to the case of full sky coverage.

To generate fluctuation all-sky maps (the surveys cover only part of the sky) we have created maps of the coefficients α and β, starting from the values they assume in the considered patches. In this way, we have produced maps according to HEALPix pixelization, in which we have attributed a coefficient α and β value to each map pixel. For consistency with the experimental data, the values of the parameters obtained from the observations have been assigned to the pixels that correspond to the centres of the patches extracted from the surveys. The map resolution is about $3.5'$ corresponding to a map at $n_{side} = 1024$.

The choice of the value of β to be assigned to each pixel has been carried out using an algorithm of random number generation according to a uniform distribution, with null mean and unit variance. For the values of α, we have adopted two different ways, first exploiting a correlation with the coefficient β, and then making use of a generation of random numbers according to a Gaussian distribution. The details of the methods used to produce these maps are described here below.

- **step 1: "rescaling" the coefficient α**

  First of all, the coefficient α have been rescaled to their intrinsic value (different from the observed one because of Faraday depolarization) using the relation

  $$C_l^{obs} \simeq C_l^{intr} \left[\frac{\sin(\lambda^2 RM)}{\lambda^2 RM} \right]^2 ;$$

  this means an amplification factor C_l^{intr}/C_l^{obs} equal to 1.0184, 1.0115, and 1.1738 for D97, D99, and U99 surveys at the central frequencies of 2.417, 2.695, and 1.4 GHz, respectively. Of course, we have also taken into account the intrinsic synchrotron frequency dependence, approximated assuming a power law

  $$C_l \propto \nu^{-5.8} \tag{6}$$

  in order to rescale the survey and the correspondent C_ls from 2.417 and 2.695 GHz (respectively for D97 and D99) to the frequency proper of the low resolution Galactic synchrotron signal map, i.e. at 1.411 GHz (U99, by itself, is a survey realized at 1.4 GHz). Tab. 1 reports the final values of the α coefficients after multiplying by the appropriate factors taking into account both the Faraday effect and the frequency dependence.

- **step 2: filling of the map of β at $n_{side} = 1024$ with experimental data**

  In order to obtain reliable high resolution maps on the basis of data taken from experimental obsevations, we have attributed to the pixels of a map at $n_{side} = 1024$ corresponding to the central points of the patches extracted from D97, D99, and U99 the values of β found by Baccigalupi et al. 2001 fitting the C_l with the power law of Eq. 5.

- **step 3: filling of the map of β at $n_{side} = 8$ with experimental data**

  Then, we have generated a map at $n_{side} = 8$ (null anywhere except for the pixels corresponding to the central points of each $10^\circ \times 10^\circ$ patch of which the best fit law of the polarized intensity power spectrum was known), similarly to what we had done in the previous step for the map at $n_{side} = 1024$.

- **step 4: filling of the map of β at $n_{side} = 8$ using a uniform distribution**

  In this phase, we have attributed to each pixel still null of the map of β at $n_{side} = 8$, a value randomly generated from a uniform distribution in the range of values of β derived from the patches:

  $$-2.46 \leq \beta \leq -1.28.$$

survey	l (deg)	α (K^2)
D97	355	7.2×10^{-4}
D97	345	9.2×10^{-4}
D97	335	3.3×10^{-3}
D97	325	7.2×10^{-4}
D97	315	2.5×10^{-3}
D97	305	9.0×10^{-4}
D97	295	7.6×10^{-5}
D97	285	1.2×10^{-3}
D97	275	1.8×10^{-2}
D97	265	9.7×10^{-4}
D97	250	4.9×10^{-4}
D97	245	1.7×10^{-3}
D99	25	7.0×10^{-3}
D99	35	5.2×10^{-3}
D99	45	1.7×10^{-3}
D99	52.5	5.7×10^{-3}
D99	60	2.8×10^{-3}
U99	50	4.8×10^{-4}
U99	146.4	4.5×10^{-2}
U99	196.8	1.6×10^{-2}

Table 1: Coefficients α obtained from the *best fit* values properly rescaled at 1411 MHz considering the Faraday effect and the synchrotron intrinsic frequency dependence (see also the text).

- **step 5: final map of β at $n_{side} = 1024$ generated with a uniform distrbution**

  During this step, for the centre of each pixel in the map at $n_{side} = 8$ we have identified the correspondent pixel in the map at $n_{side} = 1024$. To the last one, we have then attributed the value of the considered pixel in the map at $n_{side} = 8$. To any pixel that was still null in the map of β at $n_{side} = 1024$, we have then attributed the average of the values of the pixels in the map at $n_{side} = 8$ within a 20° angular radius from the considered pixel, weighted with the inverse of the distance. This was aimed to smooth the discontinuity between different regions inside the map.

- **step 6: maps of α**

  In order to generate maps of α we have followed two different approaches. In the first case, we have used a correlation found between α and β. In the second, the values attributed to the pixels in the map of α have been generated using a Gaussian random distribution.

  (i) **Map of α correlated with β**

  The comparison between the best fit values derived for the coefficients α and β of the considered patches seems to suggest a correlation between α and β that can be approximately fitted with a law of the form:

$$\log_{10} \alpha = p(0) + p(1)\beta. \tag{7}$$

The best fit values for Eq. 7 are:

$$p(0) = -5.66, \quad p(1) = -1.70.$$

Of course, since this relation between α and β is based only on a limited data sample (only 20 pairs of values), it could be not fully representative. On the other hand, it means that where the power spectrum steepens (that is the β absolute value increases), the power tends to increases (the α value increases).

To produce also maps in agreement with the above relationship between α and β, after having produced the map of β as described in previous subsections, the map of α has been generated starting from that of β and applying to it the found best fit law.

Then, we have applied a smoothing to the maps of both α and β with a Gaussian window function with FHWM= 10° to smooth the discontinuities inside the maps.

(i) **Maps of α generated from a Gaussian distribution**

In order to obtain a fluctuation model alternative to that generated through the interpolation law represented by Eq. 7, we have produced a new map of α in the same way as we had done for the map of β (see steps 2, 3, 4 and 5), but using a Gaussian random distribution, instead of a uniform one:

$$f(x) = \frac{1}{\sqrt{2\pi}\sigma} \exp\left[-(x-\mu)^2/2\sigma^2\right],$$

where $x = \log \alpha$, μ is the mean value and σ the variance of the distribution. We have chosen to generate these numbers by working on the distribution the decimal logarithm of α instead of α itself, being the order of magnitude α really important: as a matter of fact, α is a multiplicative factor providing information on the power of the angular power spectrum C_l, and, according to the data, covers a range of many orders of magnitude.

The mean value μ of the distribution has been chosen in order to link up the angular power spectrum C_l at the value it assumes at $l = 55$, as computed from the large scale map described in Sect. 2.4; for β, we have assumed the mean value from the final map of β, to which the Gaussian smoothing with FWHM=10° had already been applied (see previous step). We have chosen the value $l = 55$ since it is an intermediate value between the large angular scales (on which the map obtained as described in Sect. 2.4 gives information) and the small ones. After finding from the all-sky Galactic synchrotron emission map the value of the C_ls at $l = 55$, we had:

$$\mu = \log_{10} \alpha(l = 55),$$

with

$$C_l(l = 55) = \alpha(l = 55) l^{\overline{\beta}}, \quad \text{e } \overline{\beta} \simeq -1.96.$$

As σ of the distribution we have chosen the variance of the sample of $\log_{10} \alpha$ that derives from D97, D99, and U99 (20 values on the whole). An estimate of μ and σ is given by

$$\mu \simeq -2.72 \quad \sigma \simeq 0.65.$$

In order to limit the range of values that we would have obtained from the Gaussian distribution characterized by these parameters to a range of values similar to that we found initially in the patches, we have forced the algorithm to reject the values that where more distant from the mean than 3.8σ; these values were then substituded with others, generated from the same distribution as well.

The angular power spectrum that we have obtained after summing up the small scale fluctuation from these α and β maps with the all-sky map of the synchrotron emission (see Sect. 2.4) shows a non-monotonic behaviour around $l = 100$. To remove this effect and obtain an angular power spectrum with a good agreement between the large and the small angular scales, we have generated other α maps, optimizing the mean value of the Gaussian distribution from which they were produced, without excessively straying from the "theoretical" one. In particular, since we need decreasing the power around $l = 100$, we have chosen smaller mean values for the distribution (that is, greater in absolute value). Finally, we have applied to the maps of α so obtained a smoothing with a Gaussian window function with FWHM=10°, as done for the previous maps of α and β.

3.2.2 Fluctuation maps

In order to obtain the polarized intensity fluctuation maps, we have reconstructed the angular power spectrum according to the values of the coefficients α and β of the maps generated as described in Sect. 3.2. In order to do it with a suitable but not very large number of values of β, we have divided the range of the values of β in eleven intervals of amplitude $\Delta\beta = 0.118$. Fixing $\alpha = 1$, for each central value of the β intervals, we have generated the power spectrum of the form of Eq. 5 in the range $100 \leq l \leq 3071$ (where 3071 is the maximum multipole value that can be reached for the angular power spectrum during the analysis of an $n_{side} = 1024$ fluctuation map using the software package HEALPix). For the lower multipoles, it has been necessary to use a different law; as a matter of fact, the angular power spectra written in terms of α and β derive from patches of very limited dimensions, and as a consequence, they do not allow an accurate reconstruction of the angular power spectra, but for the high multipoles. Besides, the choice has been due to the necessity to avoid to introduce an additional power through the small scale fluctuations starting from the angular scale that correspond to $l = 100$, where the Leiden surveys make it possible to compute the angular power spectrum of the Galactic polarized synchrotron emission. We have then used a Gaussian law:

$$C_l(l) = k\frac{1}{\sqrt{2\pi}\sigma}\exp\left[-(l-\mu)/2\sigma^2\right],$$

with $k = 1$, $\mu = 100$, $\sigma = 20$, and the condition that the linking up between this spectrum and the one obtained from the power law as a function of β ($\alpha = 1$) occurs at $l = 100$.

In correspondence to each angular spectrum so created for each of the eleven central values of the β intervals, we have generated a polarized intensity fluctuation map using the program *synfast* of the software package HEALPix.

On the basis of the β value assumed by each pixel of the map created at $n_{side} = 1024$ as described in Sect. 3.2, we have then reached the value assigned to the same pixel in the correspondent fluctuation map, obtaining, in this way, a small scale fluctuation map, at high resolution ($l_{max} = 3071$, $n_{side} = 1024$, pixel dimension $\simeq 3.5'$), where the value of the multiplicative constant was still equal to 1. Since the following relation holds:

$$\delta T_l \propto \sqrt{C_l}$$

the final fluctuation map has been multiplied by the square root of the maps of the coefficients α, generated in the two ways described above: according to the correlation represented by Eq. 7, and from a Gaussian distribution, first with mean $\mu \simeq -3$, and then with $\mu \simeq -4$ (the meaning of considering two different values of μ will be clarified later on, see Sect. 4). In this way, three different small scale fluctuation maps were available, to be summed, then, to the large scale Galactic synchrotron map.

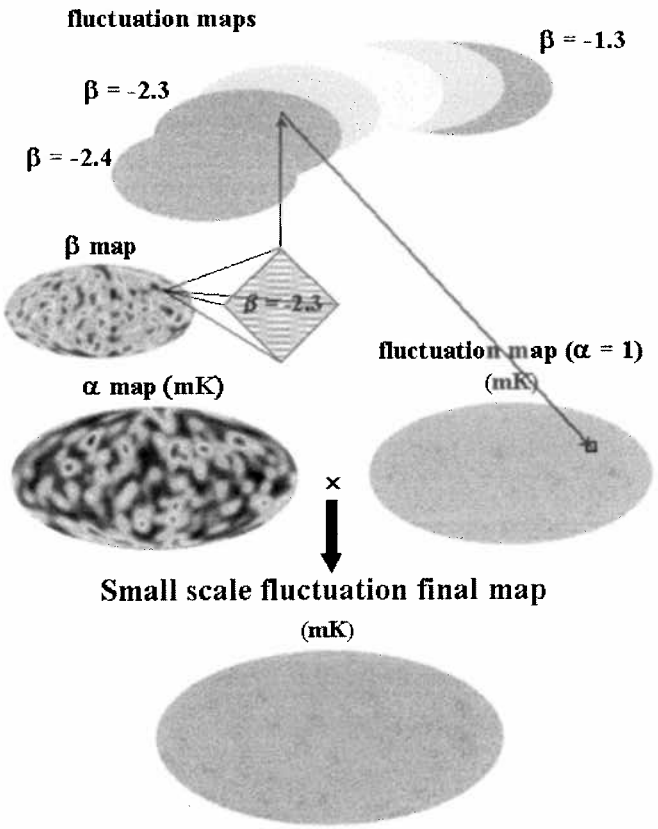

Figure 4: The figure shows the procedure followed to generate the small scale fluctuation maps from the maps of the coefficient α and β (see also the text).

3.2.3 Non Gaussianity

The program *synfast* of the HEALPix package, starting from the C_l, generates the $a_{l,m}$ coefficient of the spherical harmonics of the angular power spectrum, distributing them in a Gaussian way, in order to produce the corresponding maps of temperature or polarization (according to the specific case) fluctuations. One of the fundamental characteristics of the fluctuations that are produced in this way is the fact that their distribution on the celestial sphere is strictly Gaussian.

In order to introduce non-Gaussianity also on small angular scales, in addition to that already present in the map on large scales based on the Leiden surveys, we have reduced the interval where the distribution of the fluctuations obtained as described in Sect. 3.2 had negative values; in detail, we have renormalized the negative tail of the small fluctuation distribution by a multiplicative factor such that the most negative value have become equal, in absolute value, to the minumum of the final all-sky map of the Galactic synchrotron emission.

This kind of "de-Gaussianization" of the fluctuation maps has been applied both to the map obtained from the correlation of Eq. 7, and to the map generated from the α coefficients obtained from the Gaussian distribution with mean $\mu \simeq -3$. Eventually, four types of small scale fluctuation maps were available:

1. fluctuations generated according to the correlation of Eq. 7, with a Gaussian distribution (from now on, this case will be referred to as *corr-Gauss* model);

2. fluctuations generated according to the correlation of Eq. 7, with a non-Gaussian distribution (from now on, this case will be referred to as *corr-deGauss* model);

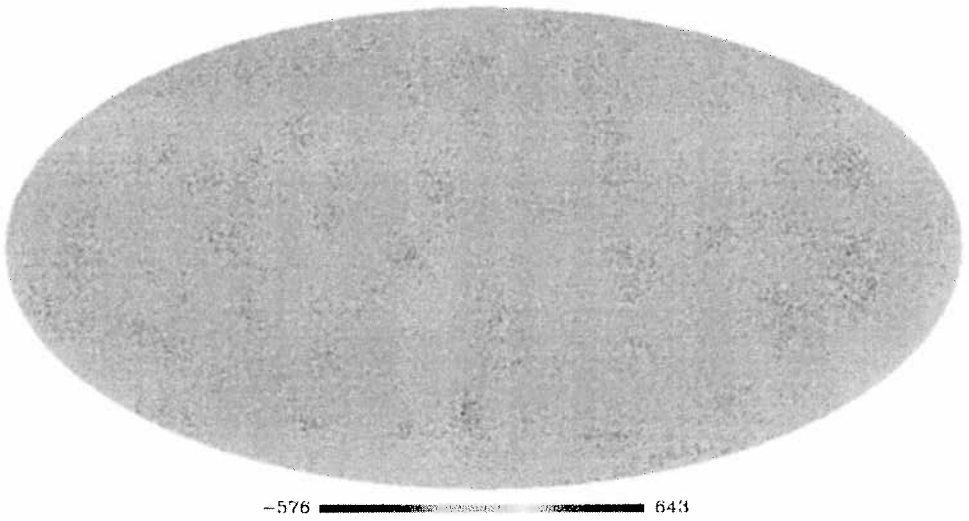

Figure 5: Small scale fluctuation map of the polarized Galactic synchrotron emission at 1.4 GHz simulated on the whole sky, at $n_{side} = 1024$, according to the *corr-Gauss* model.

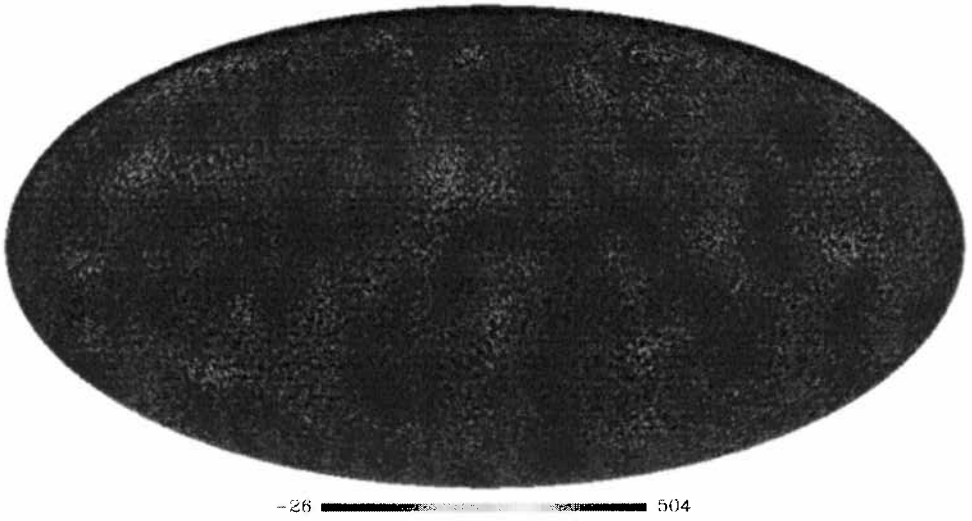

Figure 6: The same as in Fig. 5 but for the *gauss-deGauss* model.

3. fluctuations generated using a Gaussian distribution for α (in the case with $\mu = -4$), distributed in a Gaussian way (from now on, this case will be referred to as *Gauss-Gauss* model);

4. fluctuations generated using a Gaussian distribution for α (in the case with $\mu = -3$), distributed in a non-Gaussian way (from now on, this case will be referred to as *Gauss-deGauss* model).

4 Final maps of Galactic polarized synchrotron emission

The small scale fluctuation maps obtained as described in Sect. 3.2 have been then summed to the all-sky map of polarized synchrotron signal (with resolution correspondent to $n_{side} = 1024$) generated before, which provides information on the large angular scales. At the end, we generated four different models of Galactic synchrotron polarized emission.

The angular power spectra of the final maps (sums of small and large scale fluctuations) showed, when represented in a logarithmic basis, different slopes according to the adopted model. Tab. 2 reports the spectral indices relative to the angular power spectra of the different small scale fluctuation models in the range $100 \leq l \leq 3071$.

In particular, it is worth to note that the case of the *corr-Gauss* model shows, around $l = 100$, a little but abrupt, rise of the power, after which the spectrum goes on similarly to the previous multipoles, analogously to the initial *Gauss-Gauss* cases (see Sect. 3.2). While in the *Gauss-Gauss* models this could be removed with an appropriate choise of the mean value of the Gaussian distribution from which the α coefficient were generated, in the *corr-Gauss* model it was substantially weakened after the "de-Gaussianization" process described in Sect. 3.2. Interesting is, in this sense, considering the average ratio between the C_ls ($l \geq 100$) obtained from the *corr-Gauss* fluctuation model and those obtained from the *corr-deGauss* one. It results:

$$\frac{C_{l,corr-Gauss}}{C_{l,corr-deGauss}} \simeq 2.5.$$

On the contrary, when considering the *Gauss-Gauss* and the *Gauss-deGauss* models, the ratio is not significant. This is obvious, since the choice of the mean of the Gaussian distribution used in their elaboration was meant to obtain an angular power spectrum that showed a good agreement with that obtained from the large scale map.

Comparing the slopes obtained for the whole sky with the range of values β assumed in the considered patches, we can note that the simulated maps offer reliable and plausible results because the spectral indices of the power spectra remain within the requested range.

model	slope
corr-Gauss	-2.08
corr-deGauss	-1.99
gauss-Gauss	-2.39
gauss-deGauss	-2.13

Table 2: Spectral indices of the angular power spectra relative to the four models.

5 Discussion and conclusions

Simulation activities are extremely important in many fields related to the study of CMB polarization anisotropy. In this context, this study is mainly related to two different areas.

First of all, simulations make it possible to study in an accurate way the so-called main beam effects and the straylight effects due to Galactic emission. In experiments of linear polarimetry, the effects of the main beam distorsions are due to the configuration of the optics and of the focal plane that makes the main beam shape approximately elliptic instead of circular; besides, the deviations from the ideal behaviour of the detectors coupled to the telescope (Burigana et al. 1998) introduce a cross-polar contamination in the measurements. Theoretically, the detectors should answer to only one component of the electromagnetic field of the incoming radiation along the directions in a little solid angle from the line of sight. The detectors should measure the Stokes parameters I and Q along the main beam direction, with the polarization basis vectors chosen such that the x axis is aligned with the direction of the polarimetry. In fact, this is an ideal situation that differs from what is actually obtained. In general, the polarization measured in the sky has then to be convolved with the detector response pattern, not perfectly symmetric with respect to the polarization axis (Kraus 1986).

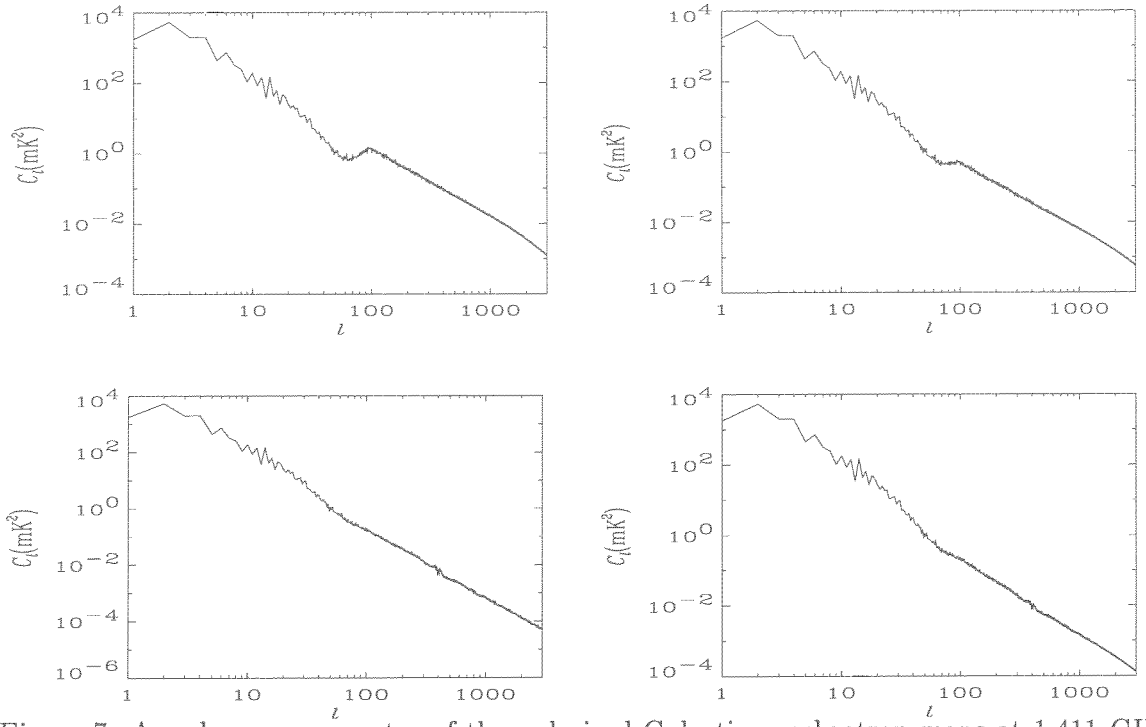

Figure 7: Angular power spectra of the polarized Galactic synchrotron maps at 1.411 GHz corresponding to our four models *corr-Gauss* (top-left panel), *corr-deGauss* (top-right panel), *Gauss-Gauss* (bottom-left panel), and *Gauss-deGauss* (bottom-right panel).

The so-called straylight contamination is the signal due to the radiation coming from directions far from the pointing direction of the beam centre angles ($\theta \gtrsim 1°$). As a matter of fact, in general, because of the effects of reflection and diffraction in the instrument, the beam pattern shows not-negligible near, intermediate and far sidelobes. As a consequence, in order to appropriately consider the straylight effect from bright sources (such as the Sun, the Moon, the Earth and the Galaxy for what concerns CMB experiments), it is necessary to know the beam pattern at low response levels ($\sim -60, -70$ dB for diffuse emissions, and $\sim -100, -120$ dB for the Solar System inner bodies), and, in the case of the diffuse components, to convolve the beam pattern on the whole sky (see, for example, Burigana et al. 2001). In order to minimize this problem, we have to operate not only on the telescope, but on the whole optical system, including the solar pannels, the shields, and the focal surface components.

On the other side, thanks to simulations, it is possible to test the quality and efficiency of various techniques designed to separate the signal from the cosmic background and from the different foregrounds, tools of crucial importance in the analysis of the maps produced from the different experiments. The most relevant foreground components are the Galactic dust, *free-free*, and synchrotron emission, fluctuations due to extragalactic (radio and Far-IR) point sources and to thermal (and marginally kinetic) Sunyaev-Zeldovich effects from clusters of galaxies.

In the case of polarization, the knowledge based on real data is currently so poor that it is not possible nor enough to fix consider unique foreground models. Extensive simulations become then necessary to optimize the instruments and the observative methodologies and the data analysis methods. This is even more important for space missions. In order to exploit as well as possible the potentialities of simulations, it is convenient to make them anchored as much as possible to the observations really available.

In the synchrotron emission simulation we have carried out, in order to exploit the available information, both at the large and at the small angular scales, we have taken into account the Leiden surveys, and the Parkes and Effelsberg surveys, respectively.

Starting from the data of the Leiden surveys, which offer a very wide sample of the sky (about the 50 %), we have simulated maps of the polarized Galactic synchrotron emission for the whole sky by implementing a geometric algorithm. From the partial coverage of the surveys, an all-sky map was generated through cycles of central symmetries. In generating the all-sky polarized synchrotron map, we have then replaced the regions with an excessive similarity with the pre-existing ones (because of the adopted algorithm), to avoid a not probable repetition of spatial structures. As a consequence, weak discontinuities are present on the borders of the substitued regions; however, they do not compromise the statistical information that can be obtained from the map.

The Parkes and the Effelsberg surveys have provided the data from which we have simulated the polarized synchrotron emission at small angular scales. From the analysis made on small patches of the sky extracted from these high resolution surveys, Baccigalupi et al. 2001 have found the best fit values for the parametrization of the synchrotron angular power spectrum for small regions in the sky, $C_l = \alpha l^{\beta}$. In order to produce the maps at a single frequency (1.4 GHz), common to the Leiden surveys and high resolution surveys, we have rescaled the best fit values of α taking into account both the depolarization due to the Faraday effect, which is mostly important at low frequencies, and the frequency dependence of the angular power spectrum, assuming a mean spectral index for the syncrotron signal in antenna temperature equal to 2.9. Then, the calculated values have been exploited to produce fluctuation maps on small scales according to four different models, paying particular attention to their more or less Gaussian character, and being careful not to add power at the $l \lesssim 100$ angular scales, where the Leiden surveys already supply information. The four models can essentially been divided in two cathegories, each with two models; in the first, there are those generated exploiting the correlation found between the best fit spectral indices β and multiplicative factors α; the second refers to fluctuations generated with α obtained from a Gaussian distribution of random numbers, with appropriate mean and standard deviation. For each cathegory, the small scale fluctuations of a model have a distribution that is intrinsecally Gaussian, while the other model shows less Gaussianity, since it is obtained from the first after rescaling the range of the negative fluctuations to lower (absolute) values.

The small scale simulated maps have been superimposed to those on large scale generated before, so producing, at the end, four different models of all-sky simulation of polarized Galactic synchrotron emission in the microwaves containing fluctuations on small and large angular scales.

Acknowledgements It is a pleasure to thank G. De Zotti and G. Giovannini for useful and constructive discussions and M. Sandri for her friendly graphical support. We acknowledge also C. Baccigalupi, L. La Porta, D. Maino, M. Maris, R. Paladini and F. Perrotta for the fruitful collaboration on this topic. The HEALPix collaboration is acknowledged.

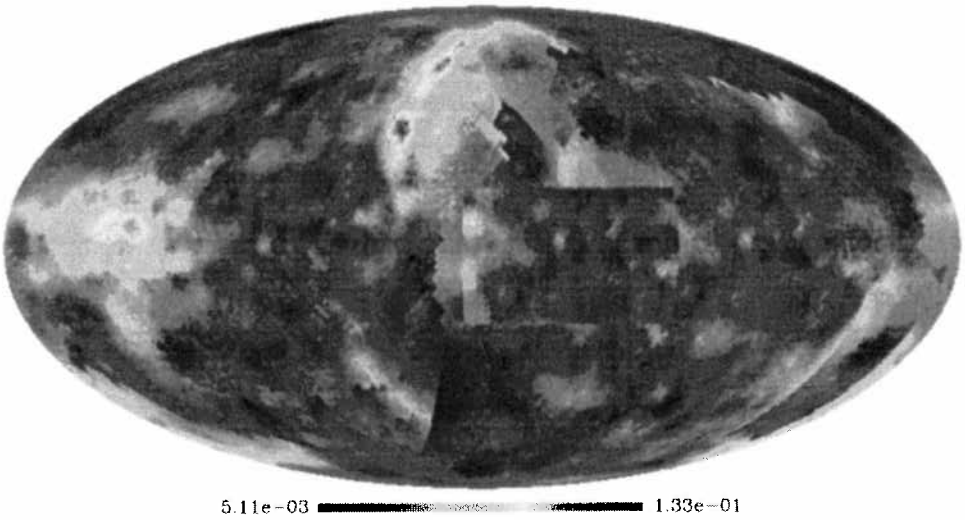

Figure 8: Map of the polarized Galactic synchrotron emission extrapolated to 30 GHz as described in the text (Sects. 2.4.3 and 3.2.1) from the map at 1.411 GHz simulated according to the *Gauss-deGauss* model.

References

[1] Baccigalupi C., Burigana C. Perrotta F. et al., A&A, **372**, 8 (2001).

[2] Burigana C., Maino D., Mandolesi N. et al., A&AS, **130**, 551 (1998).

[3] Burigana C., Maino D., Górski K.M. et al., A&A, **373**, 345 (2001).

[4] Burigana C., La Porta L., in "Astrophysical Polarized Background", Cecchini S. et al. edts., AIP Conf. Proceedings, **609**, New York (2002), pg. 54.

[5] Burn B.J., MNRAS, **133**, 67 (1966).

[6] Duncan A.R., Stewart R.T., Haynes R.F., Jones K.L., MNRAS, **277**, 36 (1995).

[7] Duncan A.R., Haynes R.F., Jones K.L., Stewart R.T., MNRAS, **291**, 279 (1997).

[8] Duncan A.R., Reich P., Reich W., Fürst E., A&A, **350**, 447 (1999).

[9] Giardino G., Banday A.J., Górski K.M., Bennett K., Jonas J.L., Tauber J., A&A, in press, astro-ph/0202520 (2002).

[10] Górski K.M. et al., software package avilable on the web site `http://www.eso.org/kgorski/healpix` (1998).

[11] Kraus J.D., *Radio Astronomy*, Cygnus-Quasar Books ed., Powell (OH) (1986).

[12] Uyaniker B., Fürst E., Reich P., Wielebinski R., A&AS, **132**, 401 (1998).

[13] Uyaniker B., Fürst E., Reich W., Reich P., Wielebinski R., A&AS, **138**, 31 (1999).